

# *The effects of variation in snow properties on passive microwave snow mass estimation*

Article

Accepted Version

Davenport, I., Sandells, M. and Gurney, R. (2012) The effects of variation in snow properties on passive microwave snow mass estimation. *Remote Sensing of the Environment*, 118 (1). pp. 161-175. ISSN 0034-4257 doi: <https://doi.org/10.1016/j.rse.2011.11.014> Available at <https://centaur.reading.ac.uk/25685/>

It is advisable to refer to the publisher's version if you intend to cite from the work. See [Guidance on citing](#).

To link to this article DOI: <http://dx.doi.org/10.1016/j.rse.2011.11.014>

Publisher: Elsevier

All outputs in CentAUR are protected by Intellectual Property Rights law, including copyright law. Copyright and IPR is retained by the creators or other copyright holders. Terms and conditions for use of this material are defined in the [End User Agreement](#).

[www.reading.ac.uk/centaur](http://www.reading.ac.uk/centaur)

**CentAUR**

Central Archive at the University of Reading

Reading's research outputs online

1 Title: The effects of variation in snow properties on passive microwave snow mass estimation

2  
3 I.J. Davenport<sup>1</sup>, M.J. Sandells<sup>1</sup>, R.J. Gurney<sup>1</sup>

4  
5 <sup>1</sup>University of Reading, Harry Pitt Building, 3 Earley Gate, University of Reading, Reading, RG6  
6 6AL, UK

7  
8 **Abstract**

9  
10 Estimating snow mass at continental scales is difficult, but important for understanding land-  
11 atmosphere interactions, biogeochemical cycles and the hydrology of the Northern latitudes.  
12 Remote sensing provides the only consistent global observations, but with unknown errors. We test  
13 the theoretical performance of the Chang algorithm for estimating snow mass from passive  
14 microwave measurements using the Helsinki University of Technology (HUT) snow microwave  
15 emission model. The algorithm's dependence upon assumptions of fixed and uniform snow density  
16 and grainsize is determined, and measurements of these properties made at the Cold Land Processes  
17 Experiment (CLPX) Colorado field site in 2002-2003 used to quantify the retrieval errors caused by  
18 differences between the algorithm assumptions and measurements. Deviation from the Chang  
19 algorithm snow density and grainsize assumptions gives rise to an error of a factor of between two  
20 and three in calculating snow mass. The possibility that the algorithm performs more accurately  
21 over large areas than at points is tested by simulating emission from a 25km diameter area of snow  
22 with a distribution of properties derived from the snow pit measurements, using the Chang  
23 algorithm to calculate mean snow-mass from the simulated emission. The snow mass estimation  
24 from a site exhibiting the heterogeneity of the CLPX Colorado site proves only marginally different  
25 than that from a similarly-simulated homogeneous site. The estimation accuracy predictions are

26 tested using the CLPX field measurements of snow mass, and simultaneous SSM/I and AMSR-E  
27 snow pit measurements.

28

29 Keywords: snow, remote sensing, passive microwave

30

## 31 **1. Introduction**

32

33 Remote sensing is the only feasible way to monitor the global distribution of snow mass, which is  
34 important for water resource management, environmental risk assessment and to determine the  
35 sensitivity of climate to change (Randall et al., 2007). Comparisons between global models,  
36 reanalysis data and satellite observations have revealed differences in distribution and magnitude of  
37 snow water equivalent (Clifford, 2010), but errors in the observations must be quantified in order to  
38 assess the accuracy of the models. Chang et al. (1987) used a simple model of soil/snow microwave  
39 emission to devise a means for estimating snow water equivalent (SWE) in mm from passive  
40 microwave measurements, by multiplying the difference between the horizontally-polarised 19GHz  
41 and 37GHz emission by a factor of 4.77, assuming snow density of  $300\text{kgm}^{-3}$ . This technique,  
42 which we refer to here as the Chang algorithm, was recommended for snow no deeper than a metre,  
43 approximately equivalent to a snow water equivalent of 300mm, due to increasing non-linearity in  
44 the relationship around this depth. The Chang algorithm has, with minor variations, been  
45 operationally used since 1987 to estimate snow mass globally from satellite observations from  
46 instruments such as SSM/I and AMSR-E.

47

48 There have been a few comparisons between snow mass measured by the Chang algorithm and by  
49 ground-based observation, showing both substantial over- and underestimation. Armstrong &  
50 Brodzik (2000) found a substantial underestimation around 20-40% in SWE when applying the  
51 Chang algorithm to snow in the former Soviet Union in the Winter 1988-89 season, for SWE

52 between 10mm and 100mm. Pardé et al. (2007) found the Chang algorithm to overestimate snow  
53 mass with an RMSE of 40mm over Winter in 2002-2003 in Central Canada, for a range of SWE  
54 between about 20mm and 150mm. They improved this to an RMSE of 12mm by incorporating a  
55 simultaneous retrieval of snow grain size into an inversion of the Helsinki University of Technology  
56 (HUT) model (Pulliainen et al., 1999). Butt (2009) demonstrated that a retrieval applying the Chang  
57 algorithm to SSM/I observations of snow in the UK with a mean depth of 90mm (so a SWE  
58 approximately 30mm), with depths up to 500mm, underestimated snow depth by a mean of 51%.  
59 He also demonstrated an approach to resolving this by a simultaneous retrieval of snow grain size,  
60 improving performance to a mean 11% overestimate. This seems to indicate a considerable range of  
61 performance of the Chang algorithm, apparently dependent upon the physical characteristics of the  
62 snow local to each study. We aim here to explore more generally the relationship between the  
63 physical characteristics of snow and the efficacy of the Chang algorithm, illustrate how simulating  
64 the retrieval can identify the flawed assumptions, and validate the approach by estimating snow  
65 mass from remotely-sensed data in an area with an extensive set of physical measurements.

66

67 By modelling the emission of microwave radiation by a snowpack and the underlying ground, we  
68 firstly test the dependence of the microwave emission of a snowpack/ground combination upon the  
69 physical characteristics of the snow, using the Helsinki University of Technology (HUT) snow  
70 microwave emission model, and use this to estimate how the Chang algorithm performance would  
71 be affected by variation in snow properties. To evaluate the effects of this variation on snow mass  
72 estimation, we also need to know how much variability in these properties is typically found in  
73 snow. We study this by using the planimetrically extensive measurements made at snow pits in the  
74 CLPX Colorado site in 2002-3. We examine how accurately the Chang algorithm would retrieve  
75 snow mass from snow with these characteristics by simulating emission with the HUT emission  
76 model driven by measured snow properties. Finally, we compare our predictions of the accuracy of

77 the Chang algorithm over the CLPX area to the application of the algorithm to SSM/I and AMSR-E  
78 measurements.

79

## 80 2. *Methods*

81

### 82 2.1. *The sensitivity of the Chang algorithm to snow grain diameter and density*

83

84 Most SWE retrievals make use of an empirical retrieval first derived by Chang et al. (1987),  
85 consisting of a linear fit to brightness temperatures at 18GHz and 37GHz, equation (1):

86

$$\text{SWE(mm)} = 4.77 (\text{TB}_{18\text{H}} - \text{TB}_{37\text{H}}) \quad \text{Equation (1)}$$

87

88 where  $\text{TB}_{18\text{H}}$  refers to the microwave brightness temperature measured at 18GHz at horizontal  
89 polarization, and  $\text{TB}_{37\text{H}}$  refers to the microwave brightness temperature measured at 37GHz at  
90 horizontal polarization. The gradient of the linear fit, in this equation 4.77, depends on the density  
91 and grain diameter of the snowpack. Whilst it is clear that a density of  $300 \text{ kg m}^{-3}$  was used to  
92 determine the gradient, the grain diameter used is uncertain. Chang et al. (1987) refer to a figure  
93 which shows brightness temperature curves as a function of SWE for two different grain radii,  
94 0.3mm and 0.5mm, and describe the algorithm as a linear fit from the data shown in the figure, but  
95 it is not clear which grain radius, or whether a combination of both, were used. Many authors (e.g.  
96 Foster et al., 1997, Kelly et al., 2003, Butt, 2009) have assumed this algorithm relates to a grain  
97 radius of 0.3mm.

98

99 To test the effect of variation in grain diameter, we use the Helsinki University of Technology  
100 emission model (Pulliainen et al., 1999) driven by a range of snow water equivalents and grain  
101 diameters to simulate emission at 19 and 37GHz,  $53^\circ$  from vertical, and apply the Chang algorithm

to estimate snow mass from this emission, indicating how the algorithm is affected by snow grain diameter. To investigate the effects of variation in snow density, we use a fixed grain diameter and range of snow water equivalents and densities, and apply the Chang algorithm to the emission to retrieve snow water equivalent. For the purposes here, some parameters have a negligible effect (Parde et al., 2007), and are kept constant, eg. soil moisture is assumed  $0.1 \text{ m}^3 \text{ m}^{-3}$ , soil temperature 272.15K, snow temperature 263.5K, and snow salinity set to zero.

## 2.2 *The dependence of snow variability on planimetric scale*

A semi-variance analysis is used to examine the characteristic length scale of variability of measured snow properties, to test for evidence that certain spatial scales are more suitable than others for averaging snow properties and estimating snow mass. It is possible that the increased variability of snow properties over large areas mean that the remote sensing relationships with areal snow mass are different, possibly better, than the relationships found at an individual field site. We attempt to identify whether the range of snow properties measured has a strong dependence upon spatial scale by geostatistical analysis of snow properties. The semivariance  $\gamma(d)$  for distance  $d$  of a set of spatially distributed measurements of  $z(\underline{x})$  is given by comparing all pairs of measurements of  $z$  separated by  $d$ , of which there are  $n(d)$ , using equation (2).

$$\gamma(d) = \frac{1}{2n(d)} \sum_{i=1}^{i=n(d)} (z(\underline{x}_i + d) - z(\underline{x}_i))^2 \quad \text{Equation (2)}$$

The NASA Cold Land Processes Experiment (CLPX) experiment produced a large number of measurements of snow properties, mass, and other variables in Colorado over 2002-2003 (Cline et al., 2002, Cline et al., 2002a, Elder et al., 2009). Figure 1 shows a map of the area of the experiment, and the locations of the main field sites. There were four Intensive Observation Periods (IOPs) during the snow seasons, over the periods February 2002, March 2002, February 2003 and

127 March 2003. Anisotropic distance semivariograms were calculated from the measurements of mean  
128 snow grain diameter in the top 5cm snow layer, snow water equivalent, snow depth, and mean snow  
129 density throughout the pack, using the North Park Meso-cell Study Area (MSA) measurements  
130 made during IOP3 over 20-23 Feb 2003. Three small intensive sets of measurements within this  
131 area were excluded from this analysis, since when analysed separately they showed semivariance  
132 consistently around double that of the rest of the measurements, suggesting a different measurement  
133 technique with a higher measurement error.

134

### 135 2.3. *Calculation of mean snow properties*

136

137 The snow pit measurements made during all four Intensive Observation Periods over the entire area  
138 of the CLPX experiment in Colorado were used to calculate the mean snow grain diameter and  
139 density within a number of SWE classes. These classes were designed to each encompass snow  
140 with a range of SWE with similar properties. Each snow pit measurement set included the minor  
141 and major axis diameters of medium size grains, and the mean of these measurements down through  
142 the snow layers is used here as representative of the site grain diameter. The depth-integrated mean  
143 snow density at each site was used to calculate the mean density within each SWE class.

144

### 145 2.4. *The effects of measured snow properties on snow mass retrieval via the Chang algorithm*

146

147 To assess the effects of measured values of density and grain diameter on the accuracy of the Chang  
148 algorithm, microwave emission at 19 and 37GHz at 53° from the vertical was simulated using the  
149 HUT model, driven by the mean snowpit measurements of SWE, density and grain diameter within  
150 the SWE classes described in Section 2.3. For each SWE class, we applied the Chang algorithm to  
151 the modelled emission, and compared the SWE estimated by the algorithm to the SWE driving the  
152 emission model. To distinguish between the effects of grain diameter and density, they were



153 separately changed within the forward model from the Chang algorithm assumptions to the  
154 measured class mean values. This demonstrates, for any given SWE, how accurately the Chang  
155 algorithm would estimate snow mass, depending on whether its assumptions of grain diameter and  
156 snow density are correct, or whether one or both more closely correspond in reality to the  
157 measurements on the CLPX site.

158

## 159 *2.5. The effect of heterogeneity in snow properties on snow mass retrieval via the Chang algorithm*

160

161 To test the hypothesis that the spatial heterogeneity in snow properties over a large area improves  
162 the accuracy of the Chang algorithm, the microwave emission from a snowpack with the  
163 distribution of SWE found within CLPX site was modelled. Having considered the case of a simple,  
164 homogeneous snowpack, where the density and grain diameter are a function of SWE in Section 2.4  
165 above, we here consider a more realistic heterogeneous snowpack, with the range of density and  
166 grain diameter occurring in the CLPX site within each SWE class. We simulated this by estimating  
167 probability density functions (PDFs) of these properties within each class, rather than, as in  
168 Section 2.4, simply using the mean of class measurements. In this case, the relationship between  
169 modelled and retrieved SWE was calculated for each class by modelling the emission for a range of  
170 density/grain diameter combinations, 20 density values between  $40\text{kgm}^{-3}$  and  $400\text{kgm}^{-3}$ , and 27  
171 grain diameter between 0.2mm and 5.4mm, and weighting the mean emission according to the  
172 PDFs. This allows us to predict for a site with any given SWE, what the algorithm estimate of SWE  
173 will be, if the site has a plausible distribution of grain diameter and density. The effect on the  
174 overall SWE estimation from a site with the distribution of SWE measured within North Park MSA  
175 during IOP3 was also calculated.

176

177 2.6. *Comparison of snow mass estimates from satellite data to ground measurements.*

178

179 We empirically tested the accuracy of the Chang algorithm by calculating the remotely-sensed SWE  
180 for the site for each of the IOPs, using the SSM/I (Brodzik, 2003) and AMSR-E (Brodzik, 2003a)  
181 measurements taken within the ground measurement time span. Armstrong & Brodzik (2001) show  
182 that reducing the brightness temperature difference in this equation by 5K provides more accurate  
183 results with SSM/I data, primarily because the algorithm was designed for 18GHz and 37GHz  
184 measurements, rather than the 19GHz and 37GHz used by SSM/I and AMSR-E, and we apply this  
185 correction in applying the algorithm.

186

187 3. *Results*

188

189 3.1. *The sensitivity of the Chang algorithm to snow grain diameter and density*

190

191 The Figure 2(a) ordinate shows the SWE used to simulate snowpack emission, the abscissa shows  
192 the SWE that would be retrieved from this emission using the Chang algorithm, and the 1:1 line  
193 represents a perfect retrieval. The retrieval which assumes a grain diameter of 0.8mm follows the  
194 perfect retrieval 1:1 line closely for low SWE, which suggests that the algorithm constant proposed  
195 in Chang et al. (1987) was chosen to work with a snow grain diameter of 0.8mm, or a radius of  
196 0.4mm, mid-way between the two radii 0.3mm and 0.5mm showed in the figure. Using  
197 Chang et al. (1987)'s Figure 1, it is easy to show that if only the 0.3mm radius emission curves had  
198 been used to calculate the constant, as has been widely assumed, the ratio between SWE and  
199  $(TB_{18H} - TB_{37H})$  would have been around 6, rather than the 4.77 given (after assuming snow density  
200 of  $300\text{kgm}^{-3}$ ), yielding SWE estimates 26% higher than an estimate based on the 0.3mm radius

assumption. The coefficient given seems to derive from the mean of the ratio between SWE and  $(TB_{18H} - TB_{37H})$  at 40cm SWE, averaged across both 0.3mm and 0.5mm snow grain radii.

Figure 2(b) shows the algorithm's sensitivity to variation in density assuming the grain diameter is fixed at 0.8mm. The effect ranges from underestimation at density of  $400\text{kgm}^{-3}$  to overestimates of a factor of six at a density of  $50\text{kgm}^{-3}$ . It can be seen that the algorithm is most accurate where the density and grain diameter exactly match the values used to formulate the algorithm, and that it starts to fail above about 150mm SWE. The suggestion in Chang et al. (1987) that the algorithm not be applied to snow depth greater than 1 meter, equivalent to approximately 300mm SWE given a snow density of  $300\text{kgm}^{-3}$ , seems to be a judgment based on the degree of acceptable error, possibly around a SWE estimation error of 10%.

The relationships between modelled and estimated SWE shown in Figure 2 strongly suggest that the Chang algorithm constant was formulated to fit snow with a grain diameter of 0.8mm, rather than the 0.6m diameter, 0.3mm radius often assumed. The impact of this misinterpretation on subsequent work is probably small, as the range of snow grainsize found in work citing it (e.g. Foster et al., 1997, Kelly et al., 2003, Butt, 2009) is far larger than this discrepancy.

### 3.2. *The dependence of snow variability on planimetric scale*

The data density in the IOP measurements allowed semivariograms with reasonable uncertainty to be calculated between lags of 5km and 25km. These showed negligible change in semivariance of mean grain diameter, density and snow water equivalent over this lag range. Mean grain diameter showed a semivariance around  $0.27\text{mm}^2$ , regardless of distance lag, suggesting a standard deviation in measurements of 0.7mm which is invariant with sample spacing within the 5km-25km range. SWE semivariance varies little from  $500\text{mm}^2$ , snow depth semivariance is around  $70\text{cm}^2$ , and mean

227 density semivariance  $3000\text{kg}^2\text{m}^{-6}$ . This suggests that heterogeneity is scale-independent over the  
228 5km-25km distance range. We have therefore not considered further the effect of spatial scale  
229 within this work, as the sampling density within these data will not provide reliable results outside  
230 this range.

231

232 The only other comparable work in geostatistical analysis of snow properties covers the northern  
233 Great Plains region of the USA (Chang et al., 2005), and indicates that ground-measured snow  
234 depth has a nugget (minimum) semivariance of about  $100\text{cm}^2$ , and reaches a sill (maximum) of  
235 approximately  $400\text{cm}^2$  at a lag of 500km. The  $70\text{cm}^2$  snow depth semivariance in the CLPX  
236 measurements indicates that they are more consistent than those taken during the Great Plains  
237 fieldwork, possibly reflecting a more accurate measurement system. Assuming this to be the case,  
238 the lack of a trend in semivariance across the 5km - 25km lag range would not be inconsistent with  
239 the semivariance behaviour within the Great Plains data, which varied little over the same distance  
240 range. The implication that might be deduced from this is that in order to estimate snow variability  
241 over a 25km scale, sampling a sub-area of 5km should prove adequate. This result may well not be  
242 globally applicable however, as the measurement sites in this experiment were of necessity close to  
243 roads rather than evenly distributed through the area, and the range of snow depth is not globally  
244 representative.

245

### 246 3.3. *Calculation of mean snow properties*

247

248 The class SWE ranges, and means of snow density and grain diameter within the classes for the  
249 observations made over Intensive Observation Periods (IOPs) 1, 2, 3 and 4 at the CLPX Colorado  
250 site are shown in Table 1, and illustrated in Figure 3. Snow water equivalent measurements were  
251 made to the nearest whole mm.

252

253 The snow properties for snow mass in the sub-300mm SWE range where we expect the Chang  
254 algorithm to be effective show considerable deviation from the values assumed in the algorithm.  
255 Whilst measurements using different techniques can give a variety of snow grain size estimates,  
256 making the absolute grain size values subject to interpretation, the considerable variability in snow  
257 grain diameter in the low SWE range should be reflected by any self-consistent measurement  
258 system. In this data, snow diameter only reaches a value consistently close to that assumed by the  
259 Chang algorithm above 300mm SWE, in a regime where the algorithm is not applied because of  
260 nonlinearity in the modelled relationship. Similarly, there is a substantial variation in the range of  
261 snow density at low SWE, mostly more than  $100\text{kgm}^{-3}$  below the  $300\text{kgm}^{-3}$  algorithm assumption.  
262 The mean snow density over all pits during IOP3 was in fact  $145\text{kgm}^{-3}$ , less than half the algorithm  
263 assumed value. This dataset has limitations, since the pit locations are of necessity close to roads,  
264 and the snow depth is relatively low, however it remains the most appropriate for this work, and  
265 similar measurements taken at Reynolds Creek Experimental Watershed over thirty years (Marks et  
266 al, 2000) show a similar relationship between density and SWE, with density about  $30\text{kgm}^{-3}$  higher  
267 than the CLPX measurements for SWE below 300mm.

268

#### 269 3.4. *The effects of measured snow properties on snow mass retrieval via the Chang algorithm*

270

271 The effect of using the mean snow grain diameter and density measurements from the CLPX site  
272 (Table 1, Figure 3) in the emission model is shown in Figure 4. The snow water equivalent used in  
273 the forward modelling is shown along the ordinate; the abscissa denotes the snow water equivalent  
274 calculated from the simulated microwave emission driven by the measured mean values of mean  
275 snow density and grain diameter. A line shows the 1:1 mapping expected if the Chang algorithm  
276 exactly calculated the snow water equivalent. The other lines show the mapping between the input

277 SWE and that derived from applying the Chang algorithm to the HUT model driven by these  
278 different assumptions of snow grain diameter and density :-

- 279 • Snow grain diameter of 0.8mm and density of  $300\text{kgm}^{-3}$ , both as assumed by the Chang  
280 algorithm
- 281 • Snow grain diameter of 0.8mm as assumed by the Chang algorithm, snow density according  
282 to the CLPX measurements in Table 1
- 283 • Snow grain diameter according to the CLPX measurements in Table 1, snow density  
284  $300\text{kgm}^{-3}$ , as assumed by the Chang algorithm
- 285 • Snow grain diameter and density both according to the CLPX measurements in Table 1.

286

287 For most of the range of SWE, the algorithm overestimates SWE by a factor of between 2 and 3.  
288 The relative effects of the deviation from the algorithm values of grain diameter and density can be  
289 seen by replacing the algorithm values used within the emission model individually. The dashed  
290 line shows that using the algorithm grain diameter of 0.8mm in the HUT model, and using only the  
291 density from the snowpit measurements gives rise to a small increase in the estimated SWE over the  
292 expected retrieval. Using the snowpit grainsize measurements with the  $300\text{kgm}^{-3}$  algorithm density  
293 in the emission model gives a far greater estimated SWE difference, indicating that the difference  
294 between the grainsize assumed in the algorithm and that measured in the snow pits is the dominant  
295 cause of this SWE over-estimation. Below 300mm SWE, the mean departure from exact retrieval  
296 caused by the CLPX-measured grain size is just over five times greater than that caused by using  
297 the CLPX-measured density.

298

299    3.5.     *The effect of heterogeneity in snow properties on snow mass retrieval via the Chang*  
300    *algorithm*

301

302    The Chang algorithm estimates of SWE from the HUT-simulated emission are shown in Figure 5,  
303    for each class for homogeneous snow, and heterogeneous snow where variability in individual pit  
304    measurements is incorporated. The mean simulated emission from the 109 North Park MSA pits  
305    measured during IOP3 would yield an overall retrieved SWE of 62.4mm assuming snow was  
306    homogeneous within the SWE classes, and 72.8mm for heterogeneous snow. The field  
307    measurements of SWE used to drive the emission model had a mean of 23.8mm.

308

309    The heterogeneity does not seem to make a significant difference, though there is an apparent  
310    reduction for SWE above 150mm. This would imply, for example, that a snow pack with a mean  
311    SWE of 200mm with the range of snow properties seen at this site for such a SWE would have a  
312    retrieved SWE of 370, whereas a snowpack with a SWE of 200mm and appropriate uniform mean  
313    properties would have a retrieved SWE around 500mm. For most of the SWE regime, this indicates  
314    that the variation in properties seen on this scale does not give rise to a substantial improvement in  
315    soil moisture retrieval from the Chang algorithm.

316

317    3.6.     *Comparison of snow mass estimates from satellite data to ground measurements.*

318

319    Whilst SSM/I measurements were available for all four IOPs, AMSR-E measurements were only  
320    available for IOPs 3 and 4. Snow liquid water content was assessed qualitatively on-site by those  
321    taking the physical measurements for a number of pits as either ‘dry’, ‘moist’ or ‘wet’, and the  
322    results are tabulated in Table 2. These indicate that during IOP2, the snow was judged to be far

323 wetter than during the other periods, and we expect the estimation accuracy to be poor in such  
324 conditions.

325

326 The snow mass estimates calculated from the satellite-measured brightness temperatures and the  
327 mean of the snow water equivalent snow-pit measurements is plotted for each IOP in Figure 6; the  
328 temporal extent of the snow-pit lines indicates the time span of the pit measurement campaign. The  
329 SWE estimates based on applying the Chang algorithm to the mean brightness temperatures during  
330 each campaign are also given in Figure 6, with the mean of the pit SWE measurements for each  
331 IOP.

332

333 These figures show an estimated mean snow mass calculated from SSM/I and AMSR-E  
334 measurements approximately twice the value measured on the ground, in line with the analysis of  
335 Section 3.4 and Figure 4. For IOP3, where AMSR-E measurements are also available, they are  
336 somewhat lower than those based on the SSM/I measurements, through it is difficult to draw  
337 conclusions from such a small set of observations. The estimation fails as expected for the IOP2  
338 measurements because the liquid water within the snow has substantially reduced penetration of the  
339 19GHz radiation through the snow pack.

340

#### 341 4. *Conclusions*

342

343 Based on the physical properties of the snow measured at the CLPX Colorado site, and the HUT  
344 microwave emission model, snow mass calculations using the Chang algorithm overestimate snow  
345 mass by a factor of two or more, predominantly because of the assumption of fixed grain diameter,  
346 which shows substantial variation in the SWE range below about 300mm where the algorithm is  
347 usable. This overestimation does not appear to be significantly affected by the heterogeneity in  
348 snow properties exhibited at the site over a 25km distance.



349

350 While the CLPX measurements only indicate the range of variation of snow properties at one site,  
351 we have no reason to believe that this site is exceptionally heterogeneous, or that the snow found in  
352 the rest of the world corresponds more uniformly to the assumptions implicit in the Chang  
353 algorithm. The SWE overestimation found by Pardé et al. (2007) in Central Canada suggests a snow  
354 pack with similar grainsize characteristics to those found at the CLPX site. While the retrieved  
355 effective grain diameter fitted in their retrieval shows a mean diameter around 3mm, between 2mm  
356 and 4.5mm, ground measurements ranged between 1.3mm and 3.2mm. The sensitivity plot  
357 Figure 2(a) indicates that the underestimates found by Armstrong & Brodzik (2000) in data from  
358 the former Soviet Union, and Butt (2009) in the UK, could be attributed to a snow grain diameter  
359 around 0.6mm.

360

361 Estimation of snow mass from its interaction with microwave radiation is strongly affected by other  
362 snow characteristics, and consequently any improvement in snow mass retrieval via passive  
363 microwave measurement will require grain size information. This could be acquired by a  
364 simultaneous retrieval from microwave observations or possibly from visible and infra-red snow  
365 surface reflectivity, which has been shown to be strongly dependent on grain diameter (Nolin and  
366 Dozier, 2000). Tedesco et al. (2007) developed an approach based on this, and using MODIS  
367 AQUA and TERRA near-infrared measurements of the CLPX area we have studied in this work,  
368 North Park MSA, estimated the grain diameter of the top snow layer with an accuracy of  
369 approximately 0.18 mm. This result should be considered in the context of the gap of a day between  
370 satellite data acquisition and ground truth due to cloud conditions, and the difference between the  
371 punctual ground measurements and the area-integrated estimates imposed by the 500m wide  
372 MODIS pixels.

373

374 While this approach will not provide explicit information on the grain diameter throughout the  
375 height of the snow pack, it is possible that a physical model of the snow pack, driven by a range of  
376 measurements such as reflectivity-derived surface grain diameter estimates from satellite  
377 instruments, and numerical weather predictions of temperature and precipitation, could provide the  
378 necessary grain size information. Improved characterisation of snow structure could be used to  
379 drive a multilayer version of the single-layer HUT model used here (Lemmetyinen et al., 2010).  
380 Such a system would serve not only to improve our ability to invert an emission model to derive  
381 snow mass from passive microwave emission, but also to indicate where the emission model, and  
382 therefore the inversion, will fail. For example, the temperature within the snow pack would indicate  
383 where melt and refreeze events are likely, flagging where the presence of ice lenses and liquid water  
384 will cause problems for the emission model. The dynamic relationship between the physical model,  
385 the emission model and the observations suggests the need for a data assimilation framework to  
386 improve snow mass estimation. Data assimilation can be used to provide estimates of the snow  
387 properties through physically-based simulations of the snow cover, constrained by independent  
388 remote sensing estimates of eg. the grain size. These snow properties are then used to drive a  
389 microwave emission model. Comparison between observed and simulated brightness temperatures  
390 can be used to update the state of the modelled snowpack, and should enable more accurate  
391 retrievals of snow mass.  
392

393    *Acknowledgements*

394

395    This work was funded under the National Centre for Earth Observation, Natural Environment  
396    Research Council, UK.

397

398    *References*

399

400    Armstrong, R.L. & Brodzik, M.J., (2000). Validation of passive microwave snow algorithms, Proc.  
401    IGARSS 2000, 24-28 Jul 2000, vol. 4, 1561-1563

402

403    Armstrong, R. L. & Brodzik, M. J. (2001). Recent Northern Hemisphere snow extent: A  
404    comparison of data derived from visible and microwave satellite sensors. Geophysical Research  
405    Letters, 28, 2676– 3673.

406

407    Brodzik., M.J., Editor. (2003). *CLPX-Satellite: SSM/I Brightness Temperature Grids*. Boulder, CO:  
408    National Snow and Ice Data Center. Digital Media.

409

410    Brodzik, M.J., Editor. (2003a). *CLPX-Satellite: AMSR-E Brightness Temperature Grids*. Boulder,  
411    CO: National Snow and Ice Data Center. Digital Media.

412

413    Butt, M.J., (2009). A comparative study of Chang and HUT models for UK snow depth retrieval,  
414    International Journal of Remote Sensing, Volume 30, Issue 24, 6361 – 6379

415

416    Chang, A. T. C., J. L. Foster & D. K. Hall (1987). Nimbus-7 SMMR derived global snow cover  
417    parameters, Ann. Glaciol., 9, 39-44

418

419 Chang, A. T. C., Kelly, R. E., Josberger, E. G., Armstrong, R. L., Foster, J. L., & Mognard, N. M.  
 420 (2005). Analysis of ground-measured and passive-microwave-derived snow depth variations in  
 421 midwinter across the northern Great Plains. *Journal of Hydrometeorology*, 6(1), 20–33.  
 422

423 Clifford, D. (2010). Global estimates of snow water equivalent from passive microwave  
 424 instruments: history, challenges and future developments. *International Journal of Remote Sensing*,  
 425 31(14):3707-3726  
 426

427 Cline, D., Elder, K., Davis, B.J., Liston, G.E., Imel, D., & Yueh, S.H. (2003). Overview of the  
 428 NASA cold land processes field experiment (CLPX-2002), *Proc. SPIE*, Vol. 4894, 361;  
 429 DOI:10.1117/12.467766  
 430

431 Cline, D., Armstrong, R., Davis, R., Elder, K. & Liston, G. (2002), Updated July 2004. CLPX  
 432 LSOS Snow Pit Measurements. Edited by M. Parsons and M.J. Brodzik. In CLPX-Ground: Snow  
 433 Measurements at the Local Scale Observation Site (LSOS), J. Hardy, J. Pomeroy, T. Link, D.  
 434 Marks, D. Cline, K. Elder, R. Davis. 2003. Boulder, CO: National Snow and Ice Data Center.  
 435 Digital Media.  
 436

437 Cline, D., Armstrong, R., Davis, R., Elder, K., & Liston, G. (2002a), Updated July 2004. CLPX-  
 438 Ground: ISA Snow Pit Measurements. Edited by M. Parsons and M.J. Brodzik. Boulder, CO:  
 439 National Snow and Ice Data Center. Digital Media.  
 440

441 Elder, K., Cline, D., Liston, G.E., & Armstrong, R. (2009) NASA Cold Land Processes Experiment  
 442 (CLPX 2002/03): Field Measurements of Snowpack Properties and Soil Moisture, *Journal of*  
 443 *Hydrometeorology*, 10(1), 320-329  
 444

445 Foster, J. L., Chang, A. T. C., & Hall, D. K. (1997), Comparison of snow mass estimates from a  
 446 prototype passive microwave algorithm and a snow depth climatology. *Remote Sens. Environ.*  
 447 62:132–142.

448

449 Kelly, R. E., Chang, A. T., Tsang, L. & Foster, J. L. (2003), A prototype AMSR-E global snow  
 450 area and snow depth algorithm, *IEEE Trans. Geosci. Remote Sens.*, 41(2), 230-242, doi:  
 451 10.1109/TGRS.2003.809118.

452

453 Lemmetyinen, J.; Pulliainen, J.; Rees, A.; Kontu, A.; Yubao Qiu; Derksen, C. (2010),  
 454 Multiple-Layer Adaptation of HUT Snow Emission Model: Comparison With Experimental Data,  
 455 *IEEE Trans. Geosci. Remote Sens.*, 48(7) 2781-2794, doi: 10.1109/TGRS.2010.2041357

456

457 Marks, D., Cooley, K.R., Robertson, D.C., & Winstral, A. (2000), ARS Technical Bulletin NWRC-  
 458 2000-5, August 11, 2000, Snow monitoring at the Reynolds Creek Experimental Watershed, Idaho,  
 459 USA

460

461 Nolin, A., & Dozier, J., (2000). A hyperspectral method for remotely sensing the grain diameter of  
 462 snow, *Remote. Sens. Environ.*, 74(2), 207– 216

463

464 Pardé, M., Goïta, K., & Royer, A. (2007). Inversion of a passive microwave snow emission model  
 465 for water equivalent estimation using airborne and satellite data, *Remote Sensing of Environment*  
 466 111 (2007) 346–356

467

468 Pulliainen, J. T., Grandell, J., & Hallikainen, M. T. (1999). HUT snow emission model and its  
 469 applicability to snow water equivalent retrieval, *IEEE Trans. Geosci. Remote Sens.*, 37(3), 1378-  
 470 1390, doi: 10.1109/36.763302.

471

472 Randall, D.A., & Wood, R.A., 2007, Climate models and their evaluation, in *Climate Change 2007:*  
473 *The physical science basis. Contribution of working group I to the fourth assessment report of the*  
474 *intergovernmental panel on climate change*, edited by Solomon, S. and et al., Cambridge University  
475 Press, Cambridge, UK and New York, NY, USA.

476

477 Tedesco, M., & Kokhanovsky, A. A. (2007). "The semi-analytical snow retrieval algorithm  
478 and its application to MODIS data." *Remote Sensing of Environment*, 111(2-3), 228-241.

479

Table 1. Classes defined by SWE ranges, and mean snow properties within the ranges over all pits for IOPs 1,2,3,4					
Class	SWE range (mm)		Mean density (kg/m <sup>3</sup> )	Mean grain diameter (mm)	Number of pits used
	Lower	Upper			
1	3	7	122	0.46	66
2	8	10	120	0.58	33
3	11	13	138	0.59	29
4	14	17	152	0.76	32
5	18	24	191	1.21	32
6	25	44	225	1.21	53
7	45	68	235	1.25	29
8	69	86	223	1.46	5
9	87	104	244	1.35	12
10	105	163	230	1.36	55
11	164	221	235	1.40	28
12	222	290	253	1.00	36
13	291	433	281	0.99	69
14	434	570	298	0.96	65
15	571	700	318	0.93	38
16	701	825	341	0.80	21
17	826	1029	354	0.72	11
18	1030	1282	336	0.73	6

Table 2. Snow moisture assessment as a percentage of the number of pits with an estimate.			
Period	Dry	Moist	Wet
IOP1	55%	35%	9%
IOP2	40%	10%	50%
IOP3	49%	49%	3%
IOP4	58%	42%	0%



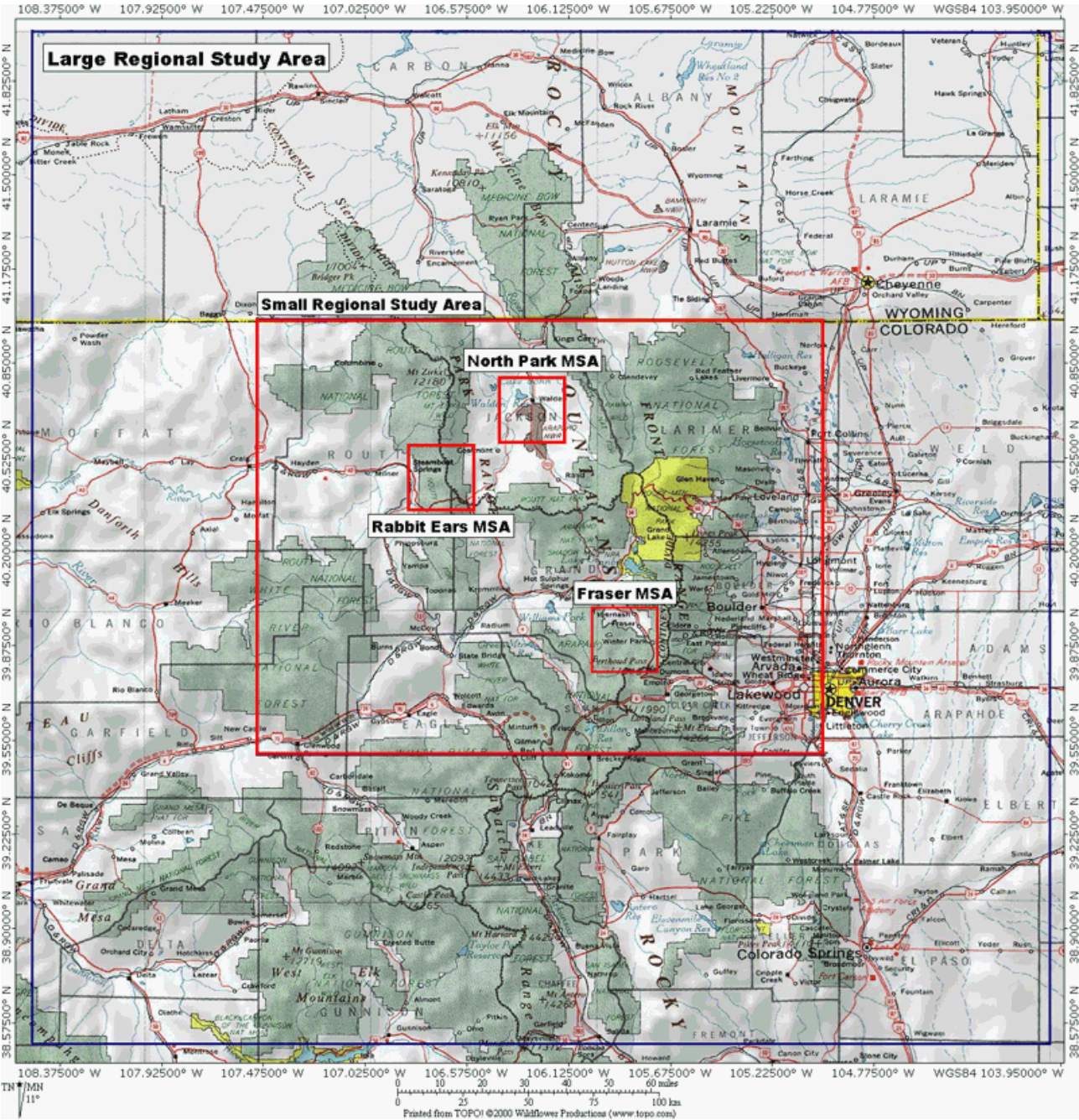


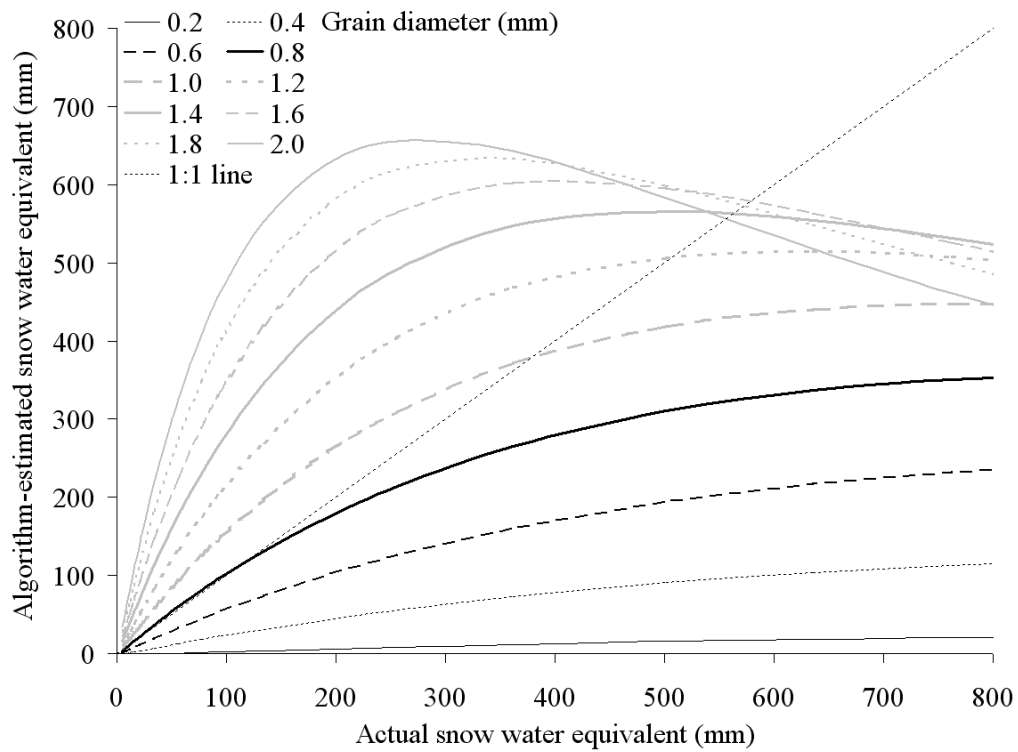
Figure 1. Nested study areas for the Cold Land Processes Field Experiment

(after <http://www.nohrsc.nws.gov/~cline/clpx.html>)

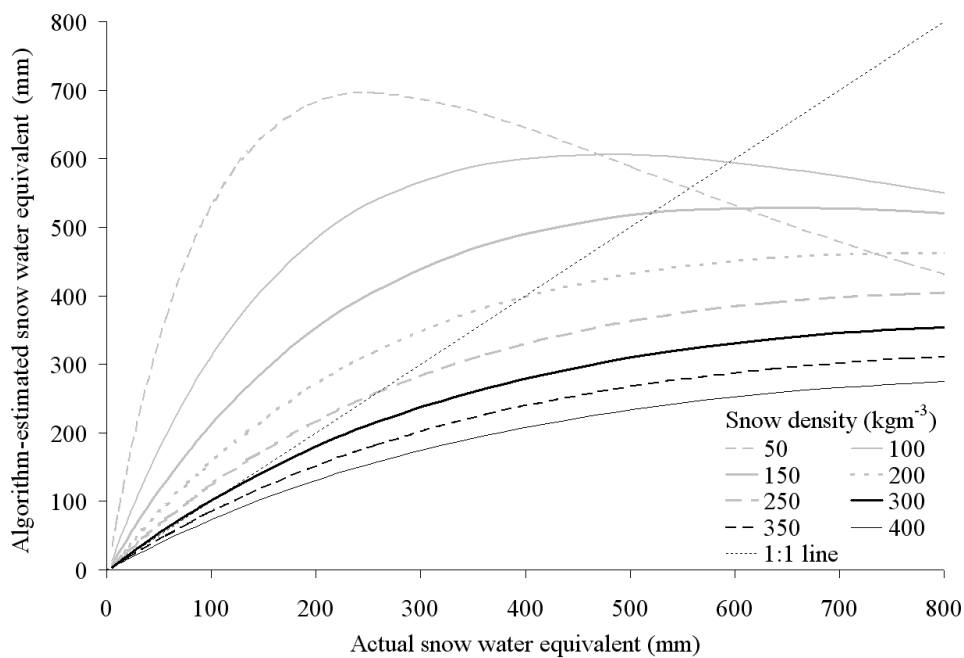
COLOUR, ONLINE VERSION



*Chang algorithm paper 2, printed Tuesday, 12 April 2011, 16:57:50, page 24 of 28*

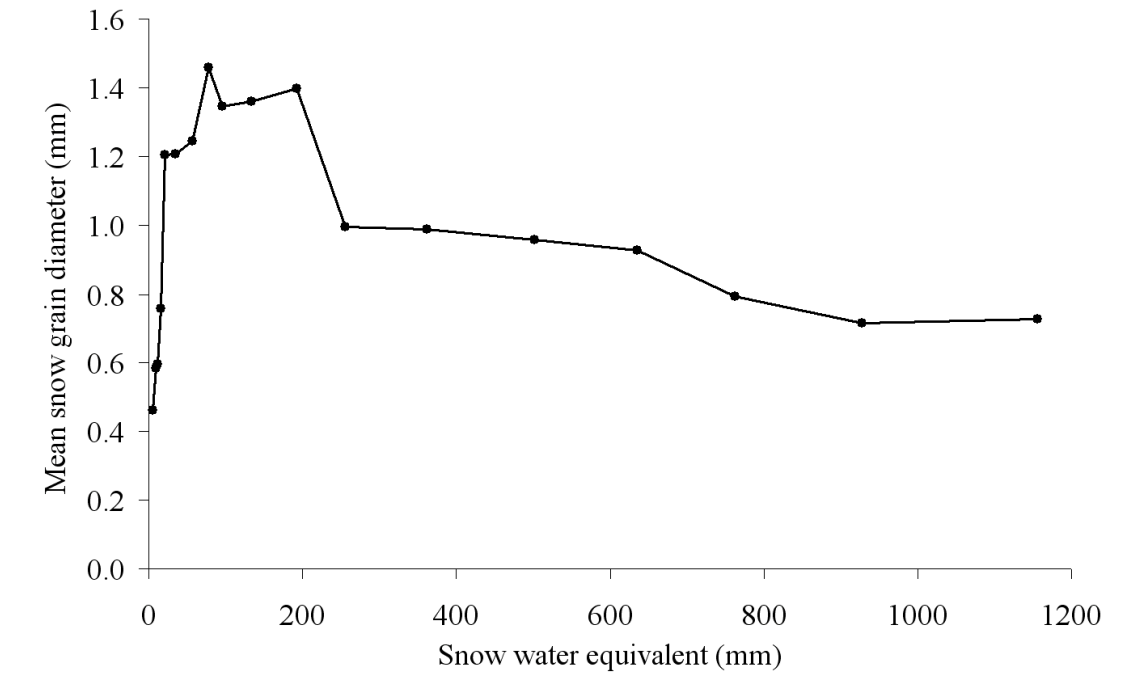


(a) Retrieval error caused by deviation of snow grain diameter from ideal value of 0.8mm while snow density is fixed at  $300 \text{ kg m}^{-3}$ .

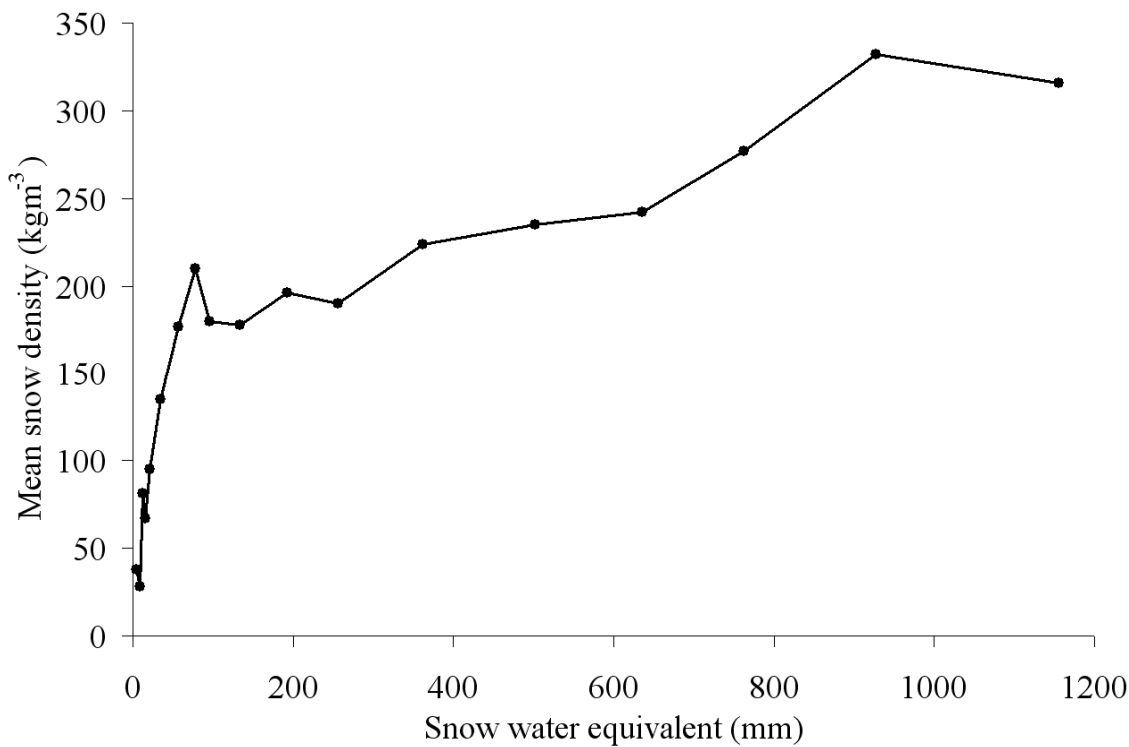


(b) Retrieval error caused by deviation of snow density from ideal value of  $300 \text{ kg m}^{-3}$  while snow grain diameter is fixed at 0.8mm.

Figure 2. Chang algorithm retrieval error caused by deviation of snow grain diameter and density from ideal values.



(a) Snow grain diameter



(b) Snow density

Figure 3. Mean snow properties within SWE classes calculated from CLPX measurements.



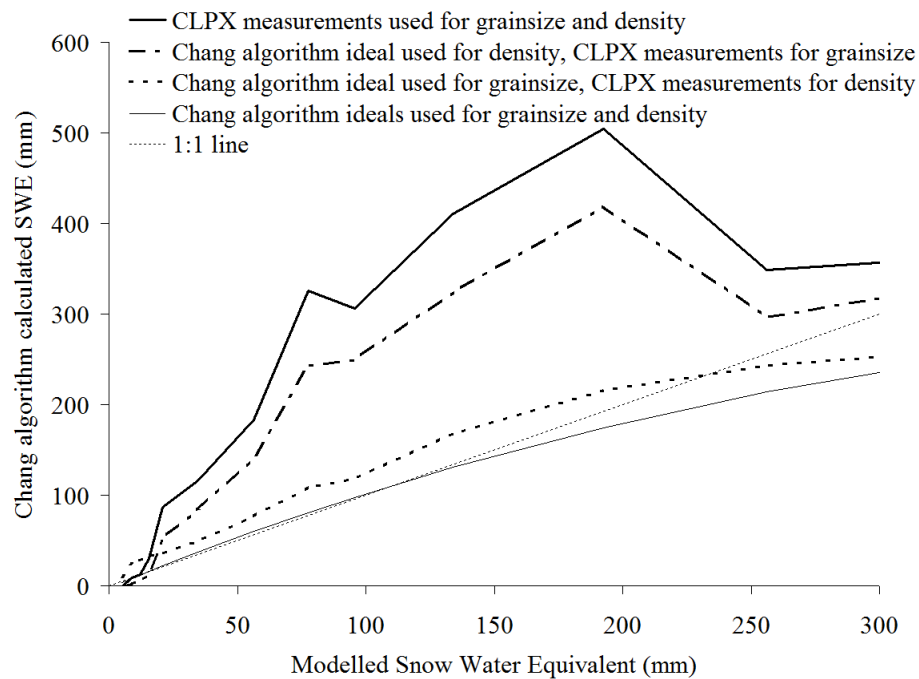


Figure 4. The effect of CLPX snow grain diameters and densities on the accuracy of snow water equivalent retrieval from the Chang algorithm, using the HUT model to calculate microwave emission.

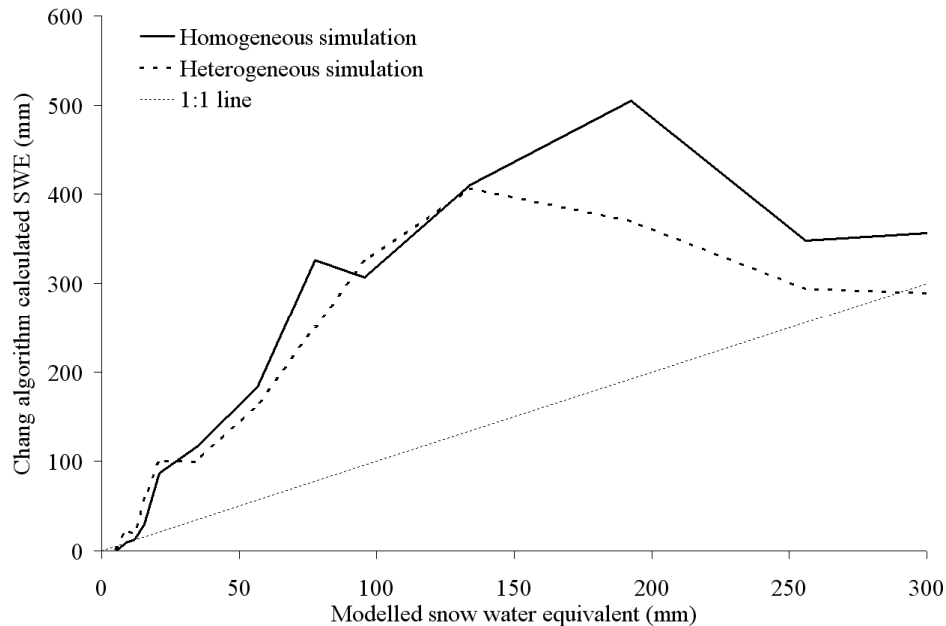
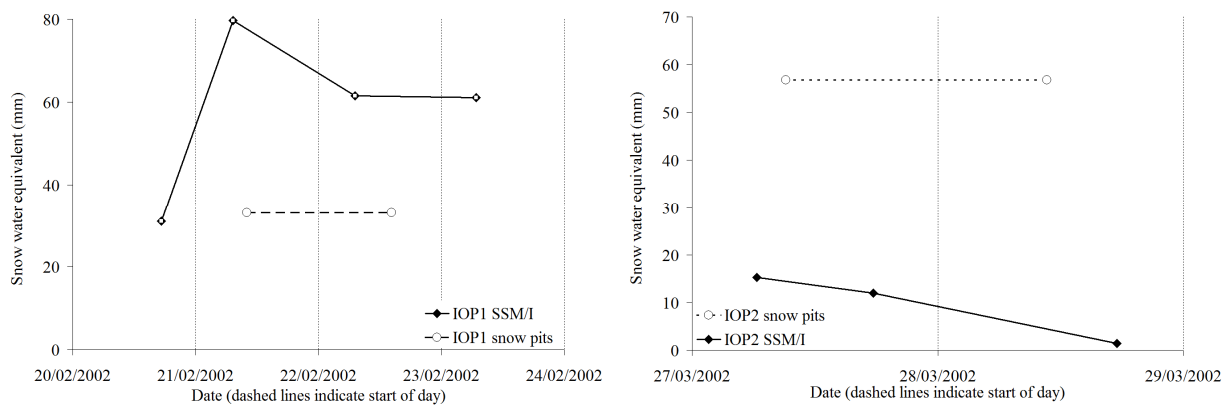
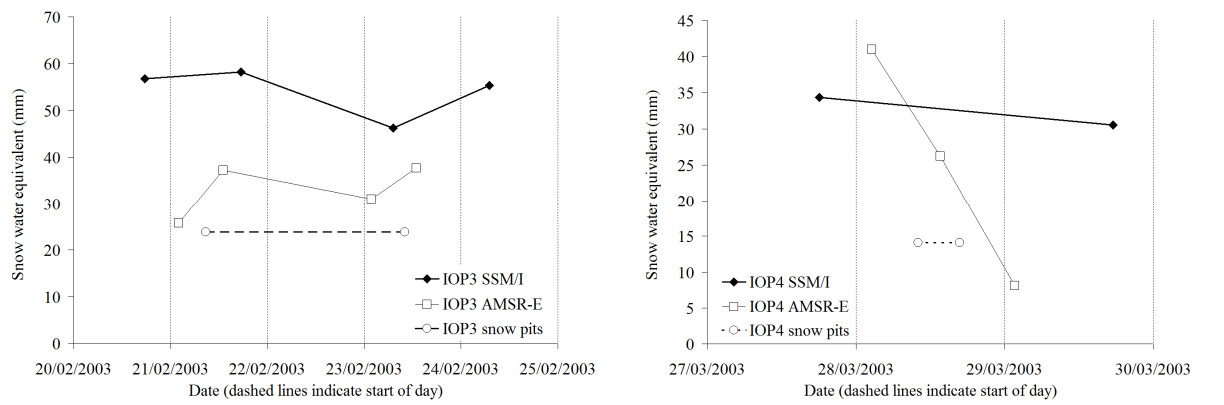


Figure 5. Snow water equivalent retrieved from microwave emission simulated by using CLPX measurements in the HUT model. Mean snow characteristics within each SWE class are used for the homogeneous line, the heterogeneous line uses a distribution of snow characteristics within each class derived from the CLPX measurements to reflect measured snow variability.



(a) IOP1, 20-24 Feb 2002, mean pit-measured SWE 33.1mm, SSM/I 70.6mm  
(b) IOP2, 27-28 March 2002, mean pit-measured SWE 56.8mm, SSM/I 9.5mm



(c) IOP3, 20-23 Feb 2003, mean pit-measured SWE 23.8mm, SSM/I 52.2mm, AMSR-E 32.9mm  
(d) IOP4, 28<sup>th</sup> March, 2003, mean pit-measured SWE 14.1mm, SSM/I 32.4mm, AMSR-E 25.1mm

Figure 6. Snow water equivalent in CLPX North Park MSA during the four Intensive Observation Periods, measured during ground campaigns and estimated from SSM/I and AMSR-E satellite data using the Chang algorithm.